# Contemporary approaches for imaging skeletal metastasis.

Ulmert, David; Solnes, Lilja; Thorek, Daniel Lj

*Published in:*
Bone Research

*DOI:*
10.1038/boneres.2015.24

2015

OPEN

Citation: Bone Research (2015) 3, 15024; doi:10.1038/boneres.2015.24
www.nature.com/boneres

REVIEW ARTICLE

# Contemporary approaches for imaging skeletal metastasis

David Ulmert[1,2], Lilja Solnes[3] and Daniel LJ Thorek[3,4]

**The skeleton is a common site of cancer metastasis. Notably high incidences of bone lesions are found for breast, prostate, and renal carcinoma. Malignant bone tumors result in significant patient morbidity. Identification of these lesions is a critical step to accurately stratify patients, guide treatment course, monitor disease progression, and evaluate response to therapy. Diagnosis of cancer in the skeleton typically relies on indirect bone-targeted radiotracer uptake at sites of active bone remodeling. In this manuscript, we discuss established and emerging tools and techniques for detection of bone lesions, quantification of skeletal tumor burden, and current clinical challenges.**

*Bone Research* (2015) **3,** 15024; doi:10.1038/boneres.2015.24; Published online: 14 July 2015

## INTRODUCTION

The treatment of a primary solid tumors may involve surgery, radiation therapy, chemotherapy, or a combination of these approaches. Treatment effectiveness and resulting survival rates are highest when the disease is still localized to the initial site. Metastatic disease, in which a malignancy has begun to spread to sites throughout the body, has more limited therapeutic options and poorer outcome. While it is difficult to generalize for the wide range of neoplastic diseases that are broadly labeled as cancer, there are several common patterns of metastatic progression. These can involve locoregional growth, spread through the lymph nodes, seeding of distant organs, and invasion of the skeleton.

The metastatic colonization of the skeleton represents the lethal form of several commonly diagnosed solid carcinomas including breast, prostate, thyroid, renal, and lung cancer. As such, it is a focus of basic biological and clinical research. Critical biological questions, such as why cancer cells have a tropism for bone, and how they are able to flourish in such a distinct microenvironment from their original soft-tissue sites, remain largely unanswered. From a clinical standpoint, detection and monitoring of bone metastasis is a key aspect of patient management in advanced disease, and will be the focus of this perspective.

### Incidence and impact

The osteotropic nature of cell dissemination from many cancers results in a large cohort number of patients with skeletal tumor burden. Estimates of approximately one-third of renal cell carcinoma patients,[1–2] as many as 70% of prostate and breast cancer patients,[3] and a large number of patients with lung,[4–5] skin,[6] and thyroid cancer[7] are affected each year. Recent assessments place the number of patients with metastatic bone disease is approximately 300 000∼400 000 in the United States alone.[8–9]

The presence and extent of bone metastases are associated with poor overall outcome in metastatic prostate, breast, kidney, and thyroid carcinoma.[10–13] Roughly four in five patients with bone metastatic breast[14] or prostate cancer[15–16] will succumb within five years. The health-care burden from this staggering number of patients is compounded by the severe health effects of bone metastasis and lack of effective treatment options. Adverse events associated with dissemination to the skeleton may include debilitating pain, fracture, hypercalcemia, and spinal cord compression.

It follows that risk stratification and patient management are intimately dependent on knowledge of the presence of bone metastasis. Clinical chemistry provides markers of skeletal metabolism that can be used for monitoring or to complement other diagnostic modalities. However, N-telopeptide, alkaline phosphatase, and

[1]Program in Molecular Pharmacology and Chemistry, Memorial Sloan Kettering Cancer Center, New York, NY, USA; [2]Department of Surgery, Skåne University Hospital, Lund, Sweden; [3]Division of Nuclear Medicine, Department of Radiology and Radiological Science, Johns Hopkins University School of Medicine, Baltimore, MD, USA and [4]Department of Oncology, Sidney Kimmel Comprehensive Cancer Center, Johns Hopkins University School of Medicine, Baltimore, MD, USA
Correspondence: Daniel LJ Thorek (dthorek1@jhmi.edu)
Received: 19 April 2015; Accepted: 23 May 2015

urine deoxypyridinoline are hampered by renal factors and are less sensitive than direct radiological evaluation of the skeleton using X-ray computed tomography (CT), magnetic resonance (MR), or nuclear medicine (NM) approaches. Therefore, imaging of bone lesions has become a mainstay of clinical radiological practice.

## IMAGING SKELETAL ACTIVITY

Tumor cell dissemination to the bone is a complex process that involves reciprocal interplay between cancer cells, cells in the surrounding microenvironment, and the stroma itself.[17] Radiographic detection of cancer metastasis to the bone is most commonly performed by identifying sites of active bone remodeling. Thus, we commonly define the bone lesions that arise as a function of the cancer/stroma interaction rather than detection of the cancer cells themselves. Chemical and physical stimuli released by metastatic foci which lead to bone deposition (as is common in prostate cancer) or resorption (as in breast cancer) have gross effects which can be visualized using several clinical imaging modalities. These methods either visualize aberrant tissue morphology (as in CT and MR) or incorporation of radiotracers in the remodeling bone matrix.

### The bone scan

The dominant approach to detect metastatic involvement of the skeleton is by a NM radionuclide bone scan (RNB) using $^{99m}$Technetium-radiolabeled bisphosphonates. Patients are scanned using a planar gamma ($\gamma$)-camera, which acquires the whole-body spatial distribution of the $^{99m}$Tc-tracer via the 140 keV $\gamma$-ray produced upon its radioactive decay. Scatter and absorption of these intermediate energy photons necessitates the collection of both anterior and posterior planar scans, which can subsequently be evaluated by a trained radiologist to identify lesions (Figure 1).

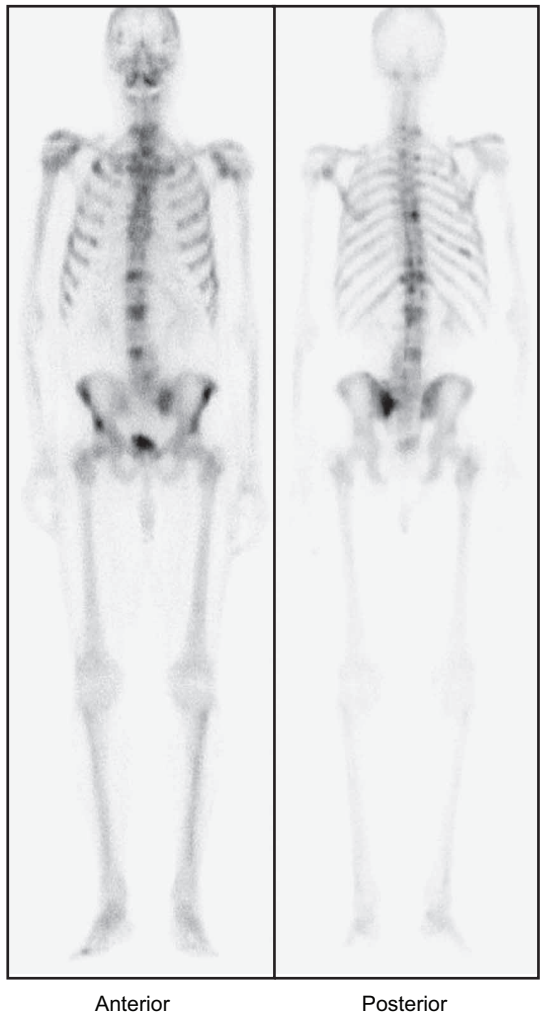


**Figure 1.** Planar bone scan. Anterior and posterior $\gamma$-camera planar scans of prostate cancer patient. Acquisition was acquired 3 hours after intravenous administration of $^{99m}$Tc-MDP. Foci of uptake of the tracer indicate lesions at thoracic and lumbar vertebrae, both shoulders and throughout the pelvis.

The $^{99m}$Tc radioisotope has been evaluated as a medical radiotracer for over half a century.[18] It is the most widely used radioisotope for medical imaging because of its ease of on-site production, facile radiolabeling chemistry (*vide infra*), favorable half-life, and image quality. $^{99m}$Tc can be produced in high quantity and purity from a $^{99}$Molybdenum ($^{99}$Mo)/$^{99m}$Technetium ($^{99m}$Tc) generator. Here, the parent $^{99}$Mo is bound to a chromatography column and decays to $^{99m}$Tc. This daughter radionuclide is mobilized with saline to produce $^{99m}$Tc pertechnetate ($^{99m}TcO_4^-$) while the $^{99}$Mo parent remains immobilized. This system obviates the need for expensive equipment such as a cyclotron (generally only found at academic hospitals) and the generator can be eluted every several hours. While concern has been mounting from the forecasted shortage of the parent $^{99}$Mo (as older research reactors which produce the isotope are decommissioned), novel cyclotron production for direct $^{99m}$Tc are expected to fill any future requirements.[19]

Several phosphate compounds have been used to complex $^{99m}TcO_4^-$ to form $^{99m}$Tc-diphosphates (Figure 2). Coordination of the radiometal with the phosphates is facile and rapid in the presence of the reducing agent stannous chloride at neutral pH. The most commonly used phosphate in the United States is medronic acid to form $^{99m}$Tc-methylene diphosphonate ($^{99m}$Tc-MDP).[20] Selection of this tracer is a function of high bone uptake, relatively quick clearance from background tissues and *in vivo* stability (both in plasma and after binding bone).[21]

Three-dimensional radionuclide distribution can be realized using single-photon emission computed tomography (SPECT). This approach rotates a number of detectors around the patient, again collecting the gamma

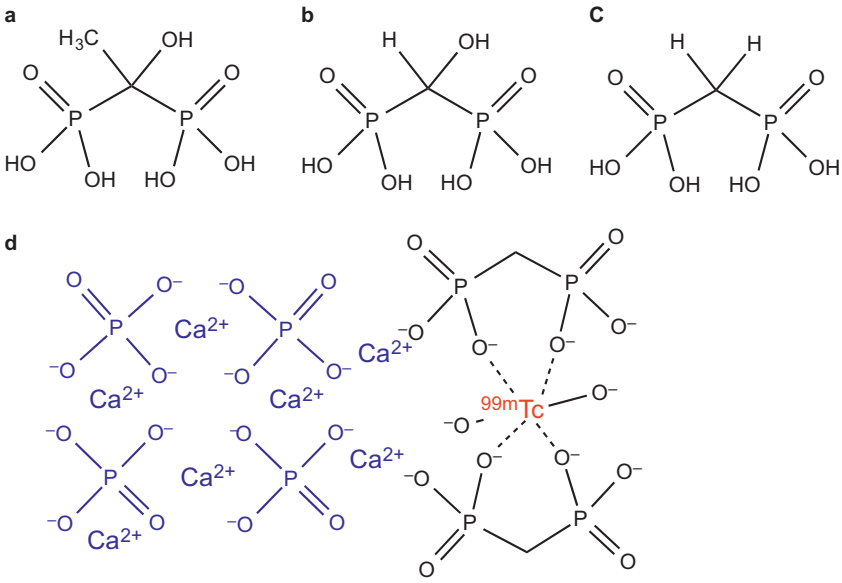


**Figure 2.** Structure and binding of bisphosphonate ligands. Several bisphosphonate compounds have been investigated for RNB, each slightly different *in vivo* binding and clearance properties. These include: (**a**) 1-hydroxy-ethylidene diphosphonate (HEBP or etidronic acid); (**b**) hydroxymethylene diphosphonate (HMDP); and the most widely used (**c**) methylene diphosphonate (MDP or medronic acid). When complexed with the single-photon emitting $^{99m}$Tc radionuclide, binding to bone is mediated by physicochemical adsorption to hydroxyapatite, shown in (**d**) for $^{99m}$Tc-MDP.

emissions, which are reconstructed to form a volumetric distribution of the tracer; as planar X-ray is to CT, γ-camera planar imaging is to SPECT. SPECT is not generally performed as a stand-alone diagnostic tool, but may be indicated following a planar RNB to clarify foci of uptake (Figure 3).

### Radiobisphosphonate uptake

All diphosphonates have a high affinity for bone mineral. Unlabeled (non-radioactive) molecules are widely used therapeutically to combat low bone density leading to osteoporotic fracture or hypercalcemia. Radiolabeled diphosphonates are given at sub-therapeutic mass doses that are assumed to function through a similar mechanism. The accumulation of these radiolabeled complexes to sites of active bone remodeling are ascribed to the coordination of the phosphate groups to the calcium present in the hydroxyapatite of bone (Figure 2d).

Uptake of these compounds appears to be multifactorial. The proliferating cells at bone metastases encourage increased vascularization and therefore increased blood flow to site. This can alter the distribution of the bone-targeted radiotracer. In elegant experiments using blood flow tracers (including radioactive microspheres and blood-dissolved radioactive gas), it has been shown that some dependence on vascular delivery rates exists. However, extraction from the vessels is not the sole component to govern uptake in both normal and newly diseased bone as diffusion and chemical adsorption play a role.[22–24] As revealed by autoradiographic development of *ex vivo* samples, bone imaging tracers incorporate at the mineralizing osteoid in developing normal bone and surrounding bone lesions.[25]

Each $^{99m}$Tc-diphosphonate possesses slightly different pharmacokinetics with respect to bone uptake and washout from background tissues[26] but can generally be used interchangeably. A general protocol sees patient imaging at approximately 3 hours after intravenous administration of approximately 600 MBq of the tracer. It should also be noted that in addition to technical artifacts, renal function, medication, and metabolic status of the patient can strongly affect scan quality and outcome.[27]

### Sodium fluoride positron emission tomography

An alternative radiotracer for imaging of the skeletal component of bone metastases is radioactive fluoride ($^{18}$F) in the form of sodium fluoride ($^{18}$F-NaF). First proposed as a RNB agent using γ-camera imaging in the 1960s, fluoride ion imaging was approved by the Food and Drug Administration in 1972. It was superseded by the widespread availability and more favorable emission profile of $^{99m}$Tc-tracers for standard sodium iodide γ-camera technology. However, the development and availability of positron emission tomography (PET) led to the rediscovery of $^{18}$F imaging for bone scanning.[28]

$^{18}$F decays primarily by positron emission. This positron undergoes an annihilation event with an electron to produce two 511 keV γ-rays which travel in opposite directions (180° from each other). Capture of dual γ-ray emissions

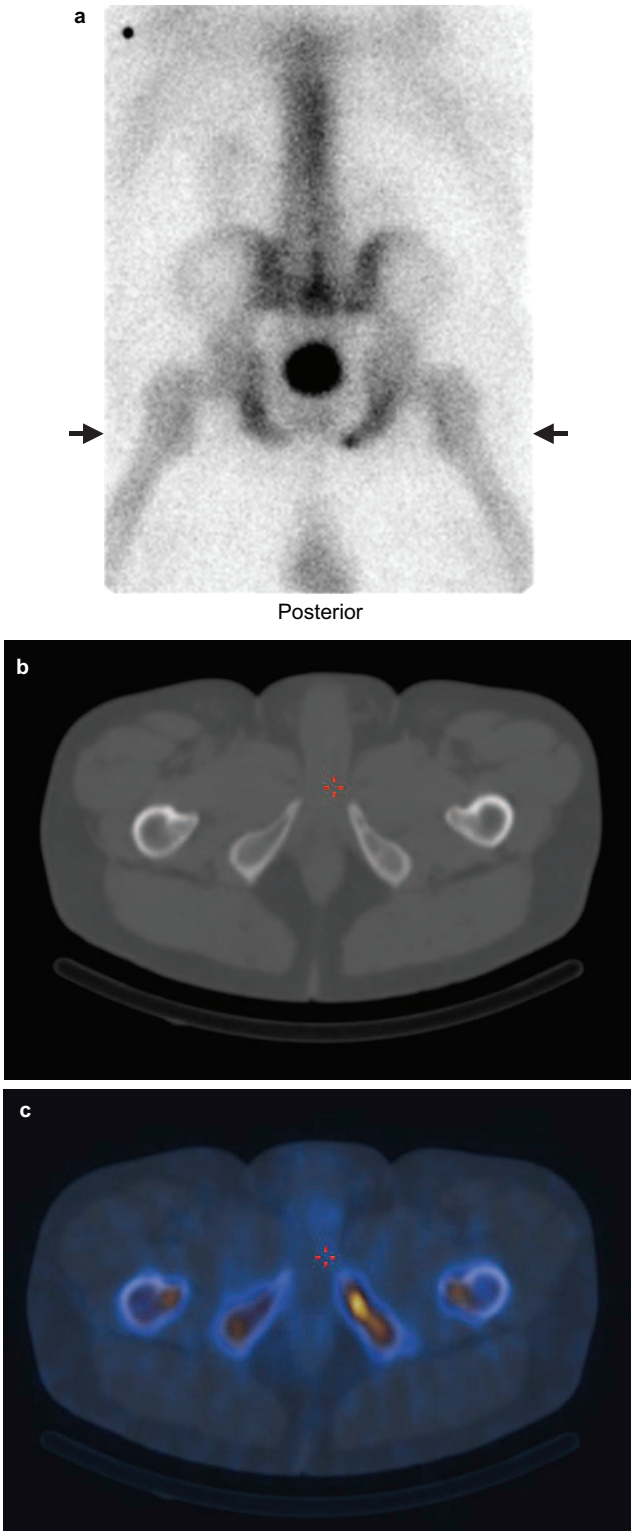


**Figure 3.** Single-photon emission computed tomography. Squat view (pelvic scan) of prostate cancer patient. There is normal, diffuse physiologic uptake in the pelvis and axial skeleton with more focal uptake in left inferior pubic ramus confirmed by follow-up pelvic SPECT/CT scan. Sclerotic lesion was identified in the same region on dedicated CT scan. Findings are compatible with osseous metastases. Intense activity in the central pelvis represents normal activity in the bladder.

which travel in opposite directions forms the basis for PET (Figure 4).[29] Here, a ring of detectors is passed over a patient injected with a positron-emitting radionuclide. Lines of response are recorded when detector elements on opposite sides of the ring are struck at the same time, and the sum of these gated events can be used to reconstruct a detailed map of the three-dimensional location of decay events.

The advantages of PET include its inherently quantitative nature, enabling the absolute determination of activity per unit volume of tissue with and a higher resolution than SPECT reconstructions of $^{99m}$Tc-diphosphonate uptake. The faster clearance of the fluoride allows for scanning earlier after injection than with $^{99m}$Tc-MDP, increasing clinical workflow and minimizing inconvenience to the patient. Additionally, PET is approximately a log-order more sensitive for radioactive detection than planar imaging or SPECT. This feature permits lower activity amounts to be administered in order to detect pathological sites and faster scan times as compared to SPECT. Importantly, PET identifies more bone metastases than the planar RNB[30] and $^{18}$F-PET/CT is able to detect more lesions than SPECT/CT.[31]

## Fluoride chemistry and bone uptake

A cyclotron is used to produce ($^{18}$F) by proton irradiation of $^{18}$O-water.[32] The fluoride ion is physicochemically adsorbed on an anion exchange resin cartridge, and can be subsequently eluted in sterile saline to form $^{18}$F-NaF. The solution is sterile filtered and calibrated for patient administration. The relatively short half-life of the radionuclide (109.7 minutes) requires that processing be performed rapidly.[33] While an on-site cyclotron is expedient, commercial services are able to produce the compound at off-site locations and deliver as needed for clinical scans.

Similar to $^{99m}$Tc-bisphosphonate compounds, uptake of $^{18}$F in regions of upregulated bone activity is dependent on several parameters.[34–35] After intravenous administration, $^{18}$F is rapidly cleared from the plasma to the bone or renally excreted.[34] The majority of bone uptake occurs on the first pass of the ion through the circulation.[36] As such, blood flow characteristics are a dominant factor in $^{18}$F-NaF uptake.[37] At metabolically active bone surfaces, the radiofluoride is able to exchange with hydroxyl ions in the hydroxyapatite crystal to form fluorapatite and fluorohydroxyapatite.[38–39] The increased mineralizing surface area at bone metastasis (as well as fracture and arthritis) result in increased $^{18}$F-fluoride uptake.[40]

## Anatomical imaging

Tracer uptake at sites of bone remodeling has critical value in detection and monitoring of bone lesions.

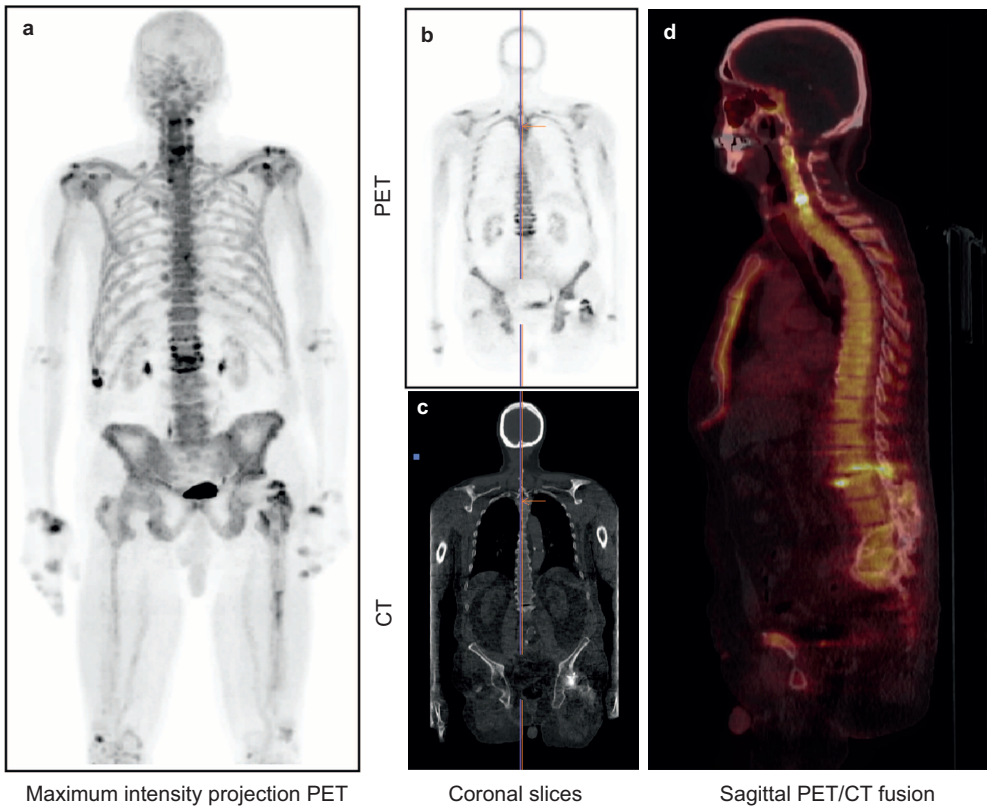


**Figure 4.** $^{18}$F-NaF PET/CT. 82-year-old patient with prostate cancer and elevated PSA who underwent an $^{18}$F-NaF PET scan. (**a**) Maximum intensity projection image (an orthographic projection of the three-dimensional data set). Multiple foci of increased uptake in the axial and appendicular skeleton detected. (**b**) PET and (**c**) CT coronal slices show selection plane for (**d**) fused PET/CT (through spine). After thorough review of the CT, most of these lesions were found to represent degenerative changes.

However, structural anatomical imaging technologies such as CT and MR imaging often provide additional information to aid diagnosis. The calcified tissue contrast of CT can be used to rule out suspicious uptake of non-metastatic origin (such as increased tracer uptake at microfractures and benign degeneration).[41] On the other hand, the excellent soft-tissue contrast afforded by MR imaging is also useful in that it may lead to identification of additional soft-tissue metastases outside of the skeleton.

Within the bone, MR is able to sensitively detect replacement of high-signal fat and marrow cellular material by incipient metastases.[42] Thus, this modality has the potential to visualize metastasis in the marrow cavity and early in the bone growth stage, prior to gross bone remodeling detectable by RNB and CT. Nevertheless, MR imaging results may again capture secondary changes in bone and bone marrow, rather than directly visualize the cancer foci itself. Early small reports on the increased sensitivity and specificity of MR and specifically whole-body MR over RNB may point to greater use of this modality for metastatic bone involvement.[43–44] These reports indicate anatomically dependent sensitivity for each modality (more rib lesions by RNB and more spinal lesions by MR) suggesting that multiple modalities might best be used in tandem. However, many centers are still in the feasibility stage for comparison of whole-body MR scanning to established techniques.[45]

## TARGETED IMAGING

Direct visualization of malignant cells rather than secondary bone events may be facilitated using NM techniques that involve the radiolabeling of targeted ligands, be they small molecules or full size antibodies. Such radiotracers facilitate detection of carcinoma through dysregulated cancer cell metabolism or aberrant cell surface receptor expression. The oncological PET tracer $^{18}$F-fluorodeoxyglucose ($^{18}$F-FDG) is the most widely used agent by a significant margin.

Malignantly transformed cells have altered metabolic requirements to furnish their high proliferation rate and altered glycolysis pathways, referred to as the Warburg effect.[46–48] This phenomenon is exploited for cancer detection using $^{18}$F-FDG, a radioglucose analog, which is trapped by phosphorylation and accumulates in cancerous tissue (Figure 5). Numerous studies have demonstrated $^{18}$F-FDG PET sensitivity and specificity for bone lesions in

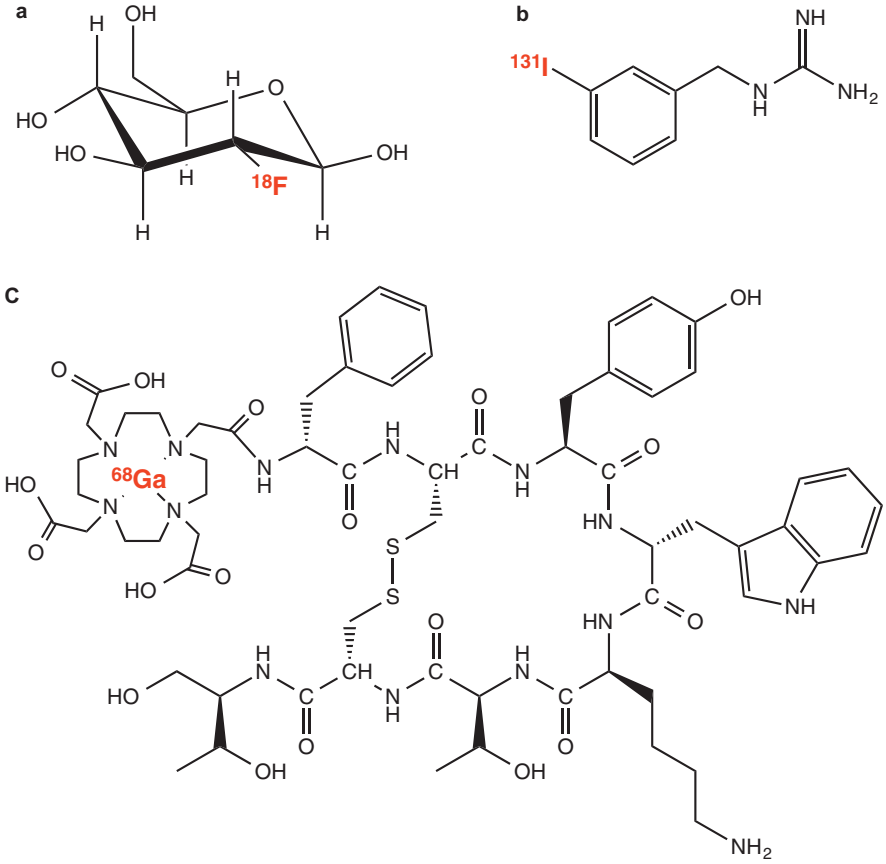


**Figure 5.** Metabolic and surface receptor-targeted agents. Many tracers are in development for direct targeted detection of cancer cells in advanced disease. Established in current clinical practice are: (**a**) $^{18}$F-fluorodeoxyglucose ($^{18}$F-FDG) which accumulates in some cancer types due to metabolic requirements; (**b**) $^{131}$I- and $^{123}$I-metaiodobenzylguanidine (MIBG) which is taken up in pheochromocytoma and neural crest tumors; and (**c**) radiolabeled somatostatin analogs (such as $^{68}$Ga-DOTATATE shown) which bind to upregulated somatostatin receptor type-2 on the cell surface.

a range of tumor types including breast,[49] lung,[50] and thyroid cancer,[51] and it may outperform traditional $^{99m}$Tc-MDP RNB in certain diseases. These results contrast with findings in a subset of less metabolically active bone lesions (including prostate and mixed osteoblastic/lytic breast cancer metastases), with subsequently lower sensitivity than planar scintigraphy.[52–54] As a result, $^{18}$F-FDG PET may best be used in conjunction with bone scans and to specifically monitor cancer cell response to treatment.[55–57]

Metabolic substrates beyond glucose have also been evaluated, most notably Carbon-11 ($^{11}$C-) and $^{18}$F-radiolabeled acetate and choline. These agents identify cancer based upon upregulated lipid synthesis and choline kinase activity, respectively. Synthesis of these compounds is more challenging than commercially available $^{18}$F-FDG, further complicated by the 20-minute half-life of the carbon isotope. Due to its reduced glycolytic phenotype, prostate cancer has been the primary application for these agents,[58] but adoption of these techniques is not currently widespread.

In addition, there are a plethora of targeting moieties that can be functionalized with single-photon and/or positron-emitting radionuclides to identify and monitor cancer. Enumerating the different agents is well beyond the scope of this article, however only a small minority are in common clinical use for detection of bone metastatic disease (Figure 6). Radioiodine (typically Iodine-131 and/or Iodine-123) is widely used for identification of differentiated thyroid metastases (which continue to accumulate iodine similar to the healthy thyroid). Peptide-based somatostatin analogs are often relied on to target neuroendocrine tumors, which overexpress somatostatin receptor type 2. These peptides are labeled with radiometals, most commonly Indium-111 ($^{111}$In) for planar imaging and SPECT,[59] and Gallium-68 for PET.[60] Finally, radioiodine-labeled MIBG has been used to identify metastatic neuroblastoma in children and malignant pheochromocytoma (Figure 7).

Many agents are in the validation stage for lesion detection in early stage clinical trials. For prostate cancer, radiolabeled urea-based small molecules and antibodies

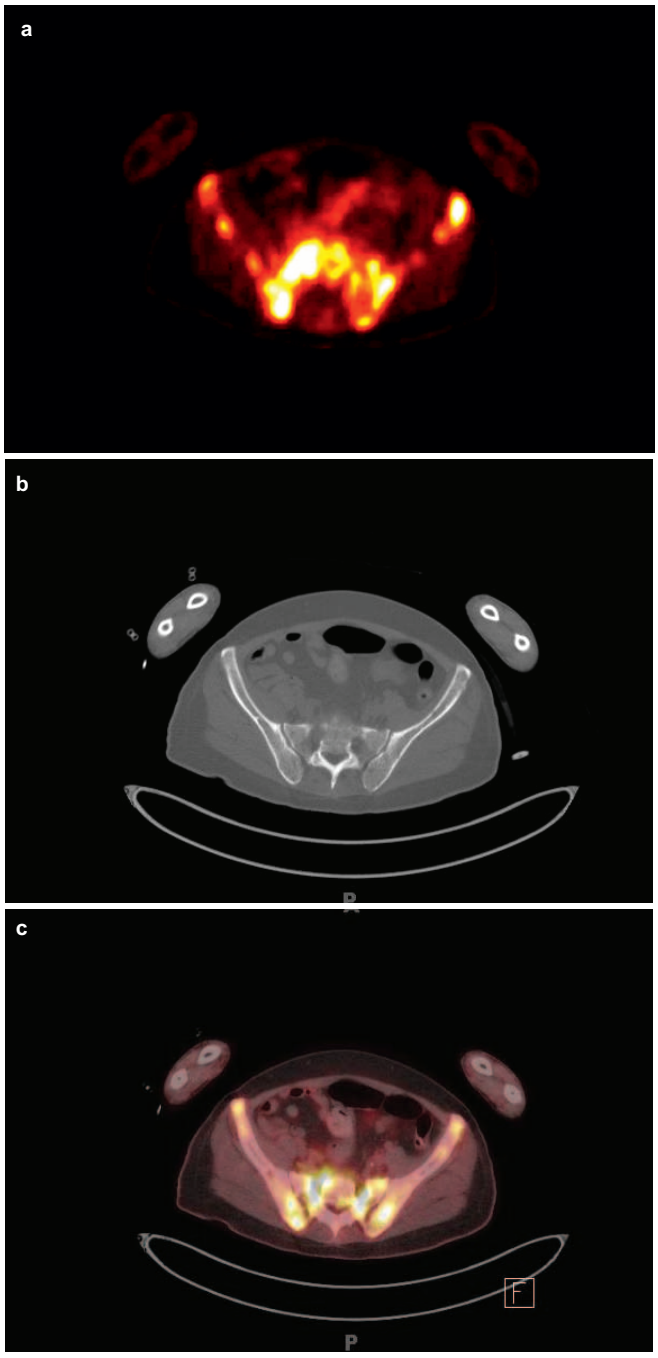


**Figure 6.** $^{18}$F-FDG PET/CT bone metastasis. $^{18}$F-Fluorodeoxyglucose (FDG) is the most widely used PET tracer. Taking advantage of the upregulated glycolytic demands of many forms of cancer, the tracer is trapped in metabolically active cells. As such, glucose-avid bone lesions can be readily identified, as seen in this lymphoma patient. (**a**) Axial $^{18}$F-FDG PET acquisition with (**b**) corresponding axial CT and (**c**) fused hybrid image. $^{18}$F-FDG uptake here is associated with subtle lytic foci compatible with metastatic disease.

targeting prostate-specific membrane antigen (PSMA) have been widely explored.[61–63] In breast cancer, radiolabeled antibodies against the overexpressed HER2/*neu* antigen have revealed primary and disseminated

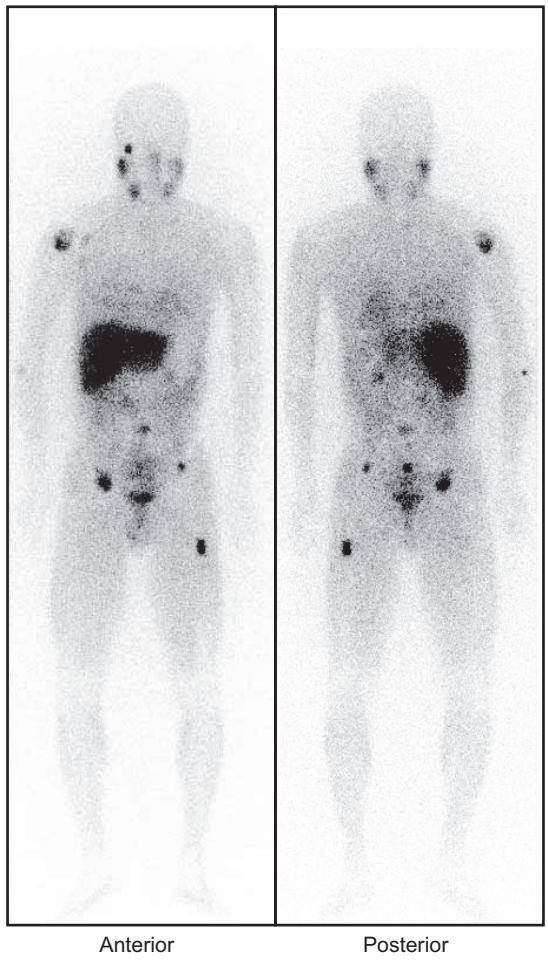


**Figure 7.** $^{123}$I-MIBG-targeted tracer uptake. Targeted imaging of metastatic pheochromocytoma with $^{123}$I-MIBG (24 hours after injection) reveals widespread metastatic disease using planar γ-camera imaging. Osseous metastases are seen in the pelvis, left femur, right orbit, and right shoulder. Normal physiologic activity is seen in the salivary glands, liver, and heart.

disease.[64] Finally, cell surface carbonic anhydrase IX (CAIX) overexpression has been targeted in renal carcinoma with $^{111}$In and iodinated anti-CAIX antibodies.[65–66] with mixed results when compared to $^{18}$F-FDG. It is expected these targeted agents, and ones like them, will have a significant future impact toward precision monitoring of disease. The slow pace of introduction of these new methods may be ascribed in part to the onerous requirements and cost of large cohort trials.

## ANALYSIS AND QUANTITATION

Qualitative evaluation of whole-body RNB or structural imaging is a relatively straightforward task that requires radiographic identification of abnormal focal uptake. Quantification of disease burden using these methods is considerably more difficult. Despite the challenge, quantitative assessment opens the opportunity to stratify

patients' disease burden, monitor progression and response to therapy, and evaluate novel cancer therapies.[67]

Ideally, rigorous and universally accepted analysis techniques are applied across patient scans to establish imaging as a biomarker to guide all relevant stages of patient assessment and management.[68] A biomarker is a factor that is objectively measured and evaluated as an indicator of normal biological processes, pathogenic processes, or pharmacologic responses to a therapeutic intervention.[69] Such an approach has been achieved with the response evaluation criteria in solid tumors (RECIST) criteria for solid tumors established in 2000.[70] In this approach, the longest axis of soft-tissue tumor burden is assessed by CT or MR and changes in this value respective to the baseline measurement define categories of outcomes. This criterion defines overall response and progression-free survival in clinical trials as an accepted imaging biomarker for the Food and Drug Administration.

However, a single one-dimensional measurement of burden is not applicable in the context of metastatic disease, and less so for bone disseminated disease. Several of the imaging methods discussed above have been evaluated for their use as imaging biomarkers. The focus for tomographic RNB as a biomarker has been has been on evaluating intensity of tracer uptake. PET is inherently quantitative, as one directly measures activity per unit volume. $^{18}$F-NaF PET uptake at a lesion is most commonly quantified as standardized uptake value (SUV), defined as the tissue concentration of tracer as measured by a PET scanner divided by the activity injected divided by body weight. The uptake value is represented by pixel or voxel intensity value in the defined volume of uptake, which is then converted into the activity concentration.

Quantification of $^{99m}$Tc-diphosphonate bone scans is more intricate. True quantification of the intensity of uptake on a planar RNB is not possible as images are formed as a projection through the patient for a given acquisition (anterior or posterior). Enumeration of the number of lesions has been historically used to evaluate planar $\gamma$-camera scans. A sophistication over this approach is the Bone Scan Index (BSI), which is an algorithm for quantitative analysis of skeletal metastasis that represents the tumor burden in a bone scan as a percentage of the total skeletal mass.[71] Although the method has shown to be of important clinical significance, popularity has been hampered by the manual labor required. Automated image analysis software has been shown to significantly decrease the time required.[72] These methods are in development and still require a physician to supervise the scan evaluation. As well, automated methods tend to underestimate BSI scores in patients with extensive bone disease.[73]

Although both BSI and quantification (SUV) of $^{18}$F PET show robust reproducibility when analyzing the same image, the intra-patient variability is currently unknown (i.e. the variability of a repeated measurement after reinjection of the compound within the same week). Future prospective clinical trials are needed to fully validate these methods as clinical applicable biomarkers.

## CURRENT CHALLENGES IN IDENTIFICATION OF BONE METASTASIS

Inherent biological and physical factors limit the effectiveness of bone metastasis imaging technologies. For the NM approaches, the complexities in analysis of patient scans arise predominantly from the difficulty in distinguishing uptake due to bone activity decoupled from cancer cell activity. Complications include benign pathologies that mimic the signal of metastatic disease, bone flare, and superscans. Anatomical imaging techniques which may detect smaller deposits of disease prior to macroscopic bone activity are also confounded by asymptomatic benign findings which often require biopsy to confirm. Together, these issues revolve around the lack of specificity of these techniques despite high sensitivity for detection of bone metabolism, which may not be associated with oncological phenomenon.

### Specificity

Cancer patients suspected of having bone disease are often elderly and present with age-associated benign skeletal degeneration. Uptake of bone-targeted radionuclides is also increased at sites of benign bone degeneration and joint inflammation.[74–76] Distinction of metastatic involvement from benign and asymptomatic bone and joint degeneration is often difficult. The intensity of radiotracer uptake may be equivalent between benign and metastatic lesions in the bone.[77–78] However, ongoing work indicates that alternative quantification criteria of lesion intensity may aid in distinction between lesions that are metastatic or merely degenerative on RNB.[79] Finally, micrometastatic lesions in the bone may not be identified since significant bone formation or resorption must occur before the lesion becomes detectable.

### Flare

The flare phenomenon refers to the increase in radiotracer uptake at previously diagnosed,[80] or new previously undetected lesions,[81] soon after initiating therapy. Increased uptake is transient, but variable, lasting between three and six months. The observation of the flare phenomenon occurs often but has been historically under-investigated.[82] It is thought that the increase is a response to bone deposition and repair at treated sites. This increase in signal makes the distinction between

progression of bone lesions (or increased metastatic spread) and successful treatment considerably difficult.

Theoretically, if all cancer burden in the bone was ablated, bone healing would continue for some time before returning to a baseline state. In such a hypothetical case, one might detect an increase in the number and intensity of bone lesions despite the lack of remaining cancer cells. Patient management in such situation is problematic as medical or radiation oncologists may be unsure if the current treatment is effective or not. Flare has been observed following systemic endocrine therapy[83–85] and chemotherapy,[86–88] as well as after focal treatment of individual sites.[89]

### Superscan

Lesions are most often identified as individual and distinct areas of intense uptake. When metastases are closely spaced, or as the area of skeletal involvement overlaps over time, it becomes difficult to identify individual sites. When the entire skeleton presents with elevated uptake, it becomes impossible to identify, enumerate or quantify the intensity of individual lesions. This so-called superscan pattern is found in advanced metastatic bone disease with diffuse activity throughout much or all of the skeleton (Figure 8). The likelihood of a superscan is increased in late stage and elderly patients with compromised kidney function, as this population is predisposed to bone metabolic disorders such as hyperthyroidism and fibrous dysplasia.[90–91]

### Pitfalls in monitoring

RNB and structural imaging are important tools to follow disease progression and response to therapy.[92] These techniques are also valuable in order to assess the potential of novel drugs – particularly as imaging response is an accepted outcome for early stage clinical trials.[93] A pitfall with monitoring of bone activity is that pleotropic drug effects on bone remodeling rather than cancer cells may be deceptive. An illustrative example is cabozantinib, a tyrosine kinase inhibitor that primarily affects hepatocyte growth factor receptor and vascular endothelial growth factor receptor. The drug is approved for treatment of medullary thyroid cancer and has shown impressive early phase results in the metastatic setting in several solid cancers. Interestingly, rapid resolution of bone lesion uptake by planar RNB was seen in advanced prostate cancer patients, with significant palliative effect.[94] Yet, the drug did not demonstrate a statistically significant benefit for overall survival.[95] This dichotomy may be explained by effects on bone turnover rather than significant anticancer impact, as suggested by resolution of $^{18}$F-PET foci at sites of tumor-free fracture in a preclinical imaging study.[96]

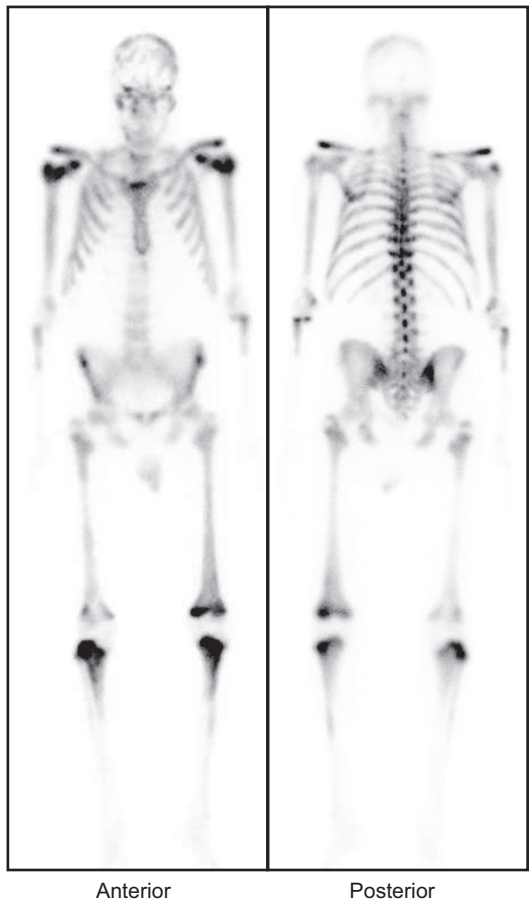


**Figure 8.** Diffuse skeletal uptake on bone scan: the superscan pattern. Anterior and posterior γ-camera planar scans with $^{99m}$Tc-MDP demonstrate diffuse uptake of tracer axial and appendicular skeleton in a patient with prostate cancer. The kidneys and soft-tissues are well visualized, however windowing of the image epitomizes the much higher skeletal uptake. These findings are consistent with a superscan pattern.

### Other concerns

Additional issues include scan duration, resolution, and artifactual uptake. From a pharmacokinetic standpoint, $^{99m}$Tc-bisphosphonates must be imaged several hours after administration to accommodate soft-tissue, serum and renal clearance of non-bone bound agent. This inconveniences the patient and requires administration of greater activity such that sufficient signal is present at the later imaging time point (thereby increasing radioactive exposure to patient and staff). Planar scintigraphy has limited resolution. Longer on-camera acquisition times are required for SPECT scans. The ability to resolve smaller sites is achieved by PET, with the trade-off of greater cost. The $^{18}$F-NaF clearance is faster and imaging can be accomplished as early as tens of minutes after administration. However the dosimetry of the positron emitting $^{18}$F does not have an advantage over $^{99m}$Tc compounds.

Reading of RNB can be complicated by soft-tissue uptake. While limited to a fraction of scans (1%–2%), uptake artifacts in the muscle and tissues often indicates the presence of pathologies such as blood flow defects, renal insufficiency, splenic uptake due to sickle cell disease or calcified soft-tissue masses.[97–99] Extraosseous uptake of $^{18}$F-NaF due to hypercalcemia, calcified soft-tissues, or common vaso-occlusion processes (such as necrosis and ischemia), are more frequently observed with this method due to the increased sensitivity of PET.

## ADVANCES

The number of targeted agents that enable precise delineation of lesions in the bone continues to increase. This progress will improve the specificity of detection and monitoring of bone tropic metastases and may help to motivate more personalized patient management. In addition, incremental improvement of existing and well-validated targeted compounds are expected to have a high impact. For example, a higher resolution and more sensitive fluorine derivate of $^{123}$I/$^{131}$I-MIBG, $^{18}$F-MFBG, has recently demonstrated impressive preclinical results of improved sensitivity to detect neuroblastoma with lower background.[100] The intense interest in targeted tracers continues to increase as new methods emerge which enable image guided-targeted focal therapy (guided external beam or surgical intervention). Many of these tracers also have theranostic potential, and can be used to identify patients, which may benefit from therapeutic derivatives of imaging compounds (for example, high-dose $^{131}$I-MIBG).

Tracer developments have been matched with advances in instrumentation and analysis methods to better quantitate and monitor disease in both patients and preclinical models. From the small animal imaging field, pinhole SPECT, and refined reconstruction algorithms now routinely enable sub-millimeter.[101–102] This technology is now being translated to the clinical arena and may enable resolution of single-photon emitters to 3 mm. Higher field-strength MR and multimodal PET/MR are also emerging with improved resolution, decreased scan time, and novel applications for fused imaging.[103] Monitoring of cancer associated bone events by RNB with the fine soft-tissue detail afforded by MR is expected to decrease false-positive lesion enumeration and improve disease monitoring. However, challenges still remain with implementation of this nascent technology with questions regarding absolute quantification, economic concerns of device cost and upkeep, and issues regarding procedure reimbursement.[104–105]

## SUMMARY

Skeletal involvement during cancer progression is directly associated with poor outcome. Effective and long-lasting treatment of disseminated bone disease remains elusive, compounding the health-care impact of this common site of metastasis. The remodeling and destruction of bone at these sites produce pain and nerve compression, fracture, and hypercalcemia which together severely impact quality of life. Methods to image the presence and track the progression of bone metastasis generally rely on indirect visualization of bone activity, primarily through radiolabeled bisphosphonates for planar scintigraphic or tomographic RNBs.

Planar RNB reveal sites of active bone remodeling associated with lesions, which can be identified and the extent of the involved skeleton quantified. Sodium fluoride PET, MR, and CT provide companion and alternative methods to detect bone involvement in advanced disease. These techniques benefit from high sensitivity for bone events but lower specificity for directly cancer-related bone involvement. This lack of specificity is a problem exacerbated by the skeletal phenotype of the elderly population that makes up the bulk of cancer patients, possessing numerous benign but degenerative bone and joint sites. Advanced methods are emerging which include disease-specific targeted imaging agents, semi-automated image processing and whole-body imaging techniques.

## Competing Interests

The authors declare no conflict of interest.

## Acknowledgements

We thank Dr. Diane Abou for the chemical structures. For funding support, we thank the Prostate Cancer Foundation Young Investigator Awards (DU and DLJT), National Institutes of Health National Cancer Institute (DU: P50-CA92629, P50-CA86438; DLJT: P50-CA058236), the Wallenberg Foundation Diagnostic Consortium Grant (DU) and the Patrick C. Walsh Prostate Cancer Research Fund (DLJT).

## References

1 Rini BI, Halabi S, Rosenberg JE *et al.* Bevacizumab plus interferon alfa compared with interferon alfa monotherapy in patients with metastatic renal cell carcinoma: CALGB 90206. *J Clin Oncol* 2008; **26**: 5422–5428.
2 Motzer RJ, Hutson TE, Tomczak P *et al.* Sunitinib versus interferon alfa in metastatic renal-cell carcinoma. *N Engl J Med* 2007; **356**: 115–124.
3 Roodman GD. Mechanisms of bone metastasis. *N Engl J Med* 2004; **350**: 1655–1664.
4 Stenbygaard LE, Sørensen JB, Olsen JE. Metastatic pattern at autopsy in non-resectable adenocarcinoma of the lung – a study from a cohort of 259 consecutive patients treated with chemotherapy. *Acta Oncol* 1997; **36**: 301–306.
5 Tsuya A, Kurata T, Tamura K, Fukuoka M. Skeletal metastases in non-small cell lung cancer: a retrospective study. *Lung Cancer* 2007; **57**: 229–232.
6 Barth A, Wanek LA, Morton DL. Prognostic factors in 1,521 melanoma patients with distant metastases. *J Am Coll Surg* 1995; **181**: 193–201.
7 Hindié E, Zanotti-Fregonara P, Keller I *et al.* Bone metastases of differentiated thyroid cancer: impact of early 131I-based detection on outcome. *Endocr Relat Cancer* 2007; **14**: 799–807.

8 Li S, Peng Y, Weinhandl ED *et al.* Estimated number of prevalent cases of metastatic bone disease in the US adult population. *Clin Epidemiol* 2012; **4**: 87–93.
9 Mundy GR. Metastasis to bone: causes, consequences and therapeutic opportunities. *Nat Rev Cancer* 2002; **2**: 584–593.
10 Carlin BI, Andriole GL. The natural history, skeletal complications, and management of bone metastases in patients with prostate carcinoma. *Cancer* 2000; **88**: 2989–2994.
11 Sathiakumar N, Delzell E, Morrisey MA *et al.* Mortality following bone metastasis and skeletal-related events among men with prostate cancer: a population-based analysis of US Medicare beneficiaries, 1999-2006. *Prostate Cancer Prostatic Dis* 2011; **14**: 177–183.
12 Manders K, van de Poll-Franse LV, Creemers GJ *et al.* Clinical management of women with metastatic breast cancer: a descriptive study according to age group. *BMC Cancer* 2006; **6**: 179.
13 Durante C, Haddy N, Baudin E *et al.* Long-term outcome of 444 patients with distant metastases from papillary and follicular thyroid carcinoma: benefits and limits of radioiodine therapy. *J Clin Endocrinol Metab* 2006; **91**: 2892–2899.
14 Coleman RE, Smith P, Rubens RD. Clinical course and prognostic factors following bone recurrence from breast cancer. *Br J Cancer* 1998; **77**: 336–340.
15 Nørgaard M, Jensen AØ, Jacobsen JB, Cetin K, Fryzek JP, Sørensen HT. Skeletal related events, bone metastasis and survival of prostate cancer: a population based cohort study in Denmark (1999 to 2007). *J Urol* 2010; **184**: 162–167.
16 Sabbatini P, Larson SM, Kremer A *et al.* Prognostic significance of extent of disease in bone in patients with androgen-independent prostate cancer. *J Clin Oncol* 1999; **17**: 948–957.
17 Nguyen DX, Bos PD, Massague J. Metastasis: from dissemination to organ-specific colonization. *Nat Rev Cancer* 2009; **9**: 274–284.
18 Sorensen LB, Archambault M. Visualization of the liver by scanning with $Mo^{99}$ (molybdate) as tracer. *J Lab Clin Med* 1963; **62**: 330–340.
19 Guérin B, Tremblay S, Rodrigue S *et al.* Cyclotron production of $^{99m}$Tc: an approach to the medical isotope crisis. *J Nucl Med* 2010; **51**: 13N–16N.
20 Chopra A. *$^{99m}$Tc-Methyl diphosphonate. Molecular Imaging and Contrast Agent Database (MICAD) [Internet]*. Bethesda (MD): National Center for Biotechnology Information, 2004.
21 Lin JH. Bisphosphonates: a review of their pharmacokinetic properties. *Bone* 1996; **18**: 75–85.
22 Riggs SA Jr, Wood MB, Cooney WP 3rd, Kelly PJ. Blood flow and bone uptake of $^{99m}$Tc-labeled methylene diphosphonate. *J Orthop Res* 1984; **1**: 236–243.
23 Lavender JP, Khan RA, Hughes SP. Blood flow and tracer uptake in normal and abnormal canine bone: comparisons with Sr-85 microspheres, Kr-81m, and Tc-99m MDP. *J Nucl Med* 1979; **20**: 413–418.
24 Sagar VV, Piccone JM, Charkes ND. Studies of skeletal tracer kinetics. III. Tc-99m(Sn)methylenediphosphonate uptake in the canine tibia as a function of blood flow. *J Nucl Med* 1979; **20**: 1257–1261.
25 Einhorn TA, Vigorita VJ, Aaron A. Localization of technetium-99m methylene diphosphonate in bone using microautoradiography. *J Orthop Res* 1986; **4**: 180–187.
26 Ogawa K, Saji H. Advances in drug design of radiometal-based imaging agents for bone disorders. *Int J Mol Imaging* 2011; **2011**: 537687.
27 McAfee JG, Singh A, Roskopf M *et al.* Experimental drug-induced changes in renal function and biodistribution of $^{99m}$Tc-MDP. *Invest Radiol* 1983; **18**: 470–478.
28 Elmaleh DR, Hnatowitch DJ, Cochavi S, McKusick KA, Brownell GL, Strauss WH. Emission tomographic images of the skull with fluorine-18. *Int J Nucl Med Biol* 1980; **7**: 289–293.
29 Phelps ME, Huang SC, Hoffman EJ, Selin C, Sokoloff L, Kuhl DE. Tomographic measurement of local cerebral glucose metabolic rate in humans with (F-18)2-fluoro-2-deoxy-D-glucose: validation of method. *Ann Neurol* 1979; **6**: 371–388.
30 Schirrmeister H, Guhlmann A, Elsner K *et al.* Sensitivity in detecting osseous lesions depends on anatomic localization: planar bone scintigraphy versus 18F PET. *J Nucl Med* 1999; **40**: 1623–1629.
31 Even-Sapir E, Metser U, Mishani E, Lievshitz G, Lerman H, Leibovitch I. The detection of bone metastases in patients with high-risk prostate cancer: $^{99m}$Tc-MDP Planar bone scintigraphy, single- and multi-field-of-view SPECT, 18F-fluoride PET, and 18F-fluoride PET/CT. *J Nucl Med* 2006; **47**: 287–297.
32 Satyamurthy N, Amarasekera B, Alvord CW, Barrio JR, Phelps ME. Tantalum [18O]water target for the production of [18F]fluoride with high reactivity for the preparation of 2-deoxy-2-[18F]fluoro-D-glucose. *Mol Imaging Biol* 2002; **4**: 65–70.
33 Garcia-Torano E, Medina VP, Ibarra MR. The half-life of 18F. *Appl Radiat Isot* 2010; **68**: 1561–1565; discussion 1565.
34 Win AZ, Aparici CM. Factors affecting uptake of NaF-18 by the normal skeleton. *J Clin Med Res* 2014; **6**: 435–442.
35 Piert M, Zittel TT, Becker GA *et al.* Assessment of porcine bone metabolism by dynamic. *J Nucl Med* 2001; **42**: 1091–1100.
36 Wootton R, Dore C. The single-passage extraction of 18F in rabbit bone. *Clin Phys Physiol Meas* 1986; **7**: 333–343.
37 Frost ML, Blake GM, Cook GJ, Marsden PK, Fogelman I. Differences in regional bone perfusion and turnover between lumbar spine and distal humerus: (18)F-fluoride PET study of treatment-naive and treated postmenopausal women. *Bone* 2009; **45**: 942–948.
38 Grynpas MD. Fluoride effects on bone crystals. *J Bone Miner Res* 1990; **5**: S169–S175.
39 Hawkins RA, Choi Y, Huang SC *et al.* Evaluation of the skeletal kinetics of fluorine-18-fluoride ion with PET. *J Nucl Med* 1992; **33**: 633–642.
40 Tomlinson RE, Shoghi KI, Silva MJ. Nitric oxide-mediated vasodilation increases blood flow during the early stages of stress fracture healing. *J Appl Physiol 1985* 2014; **116**: 416–424.
41 Love C, Din AS, Tomas MB, Kalapparambath TP, Palestro CJ. Radionuclide bone imaging: an illustrative review. *Radiographics* 2003; **23**: 341–358.
42 Vande Berg BC, Malghem J, Lecouvet FE, Maldague B. Magnetic resonance imaging of the normal bone marrow. *Skeletal Radiol* 1998; **27**: 471–483.
43 Lecouvet FE, Geukens D, Stainier A *et al.* Magnetic resonance imaging of the axial skeleton for detecting bone metastases in patients with high-risk prostate cancer: diagnostic and cost-effectiveness and comparison with current detection strategies. *J Clin Oncol* 2007; **25**: 3281–3287.
44 Venkitaraman R, Cook GJ, Dearnaley DP *et al.* Whole-body magnetic resonance imaging in the detection of skeletal metastases in patients with prostate cancer. *J Med Imaging Radiat Oncol* 2009; **53**: 241–247.
45 Iagaru A, Young P, Mittra E, Dick DW, Herfkens R, Gambhir SS. Pilot prospective evaluation of $^{99m}$Tc-MDP scintigraphy, 18F NaF PET/CT, 18F FDG PET/CT and whole-body MRI for detection of skeletal metastases. *Clin Nucl Med* 2013; **38**: e290–e296.
46 Warburg O. On the origin of cancer cells. *Science* 1956; **123**: 309–314.
47 Vander Heiden MG, Cantley LC, Thompson CB. Understanding the Warburg effect: the metabolic requirements of cell proliferation. *Science* 2009; **324**: 1029–1033.
48 Warburg O, Wind F, Negelein E. The metabolism of tumors in the body. *J Gen Physiol* 1927; **8**: 519–530.
49 Wahl RL, Cody RL, Hutchins GD, Mudgett EE. Primary and metastatic breast carcinoma: initial clinical evaluation with PET with the

radiolabeled glucose analogue 2-[F-18]-fluoro-2-deoxy-D-glucose. *Radiology* 1991; **179**: 765–770.

50 Song JW, Oh YM, Shim TS, Kim WS, Ryu JS, Choi CM. Efficacy comparison between (18)F-FDG PET/CT and bone scintigraphy in detecting bony metastases of non-small-cell lung cancer. *Lung Cancer* 2009; **65**: 333–338.

51 Ota N, Kato K, Iwano S *et al.* Comparison of (1)(8)F-fluoride PET/CT, (1)(8)F-FDG PET/CT and bone scintigraphy (planar and SPECT) in detection of bone metastases of differentiated thyroid cancer: a pilot study. *Br J Radiol* 2014; **87**: 20130444.

52 Cook GJ, Houston S, Rubens R, Maisey MN, Fogelman I. Detection of bone metastases in breast cancer by 18FDG PET: differing metabolic activity in osteoblastic and osteolytic lesions. *J Clin Oncol* 1998; **16**: 3375–3379.

53 Shreve PD, Grossman HB, Gross MD, Wahl RL. Metastatic prostate cancer: initial findings of PET with 2-deoxy-2-[F-18]fluoro-D-glucose. *Radiology* 1996; **199**: 751–756.

54 Kao CH, Hsieh JF, Tsai SC, Ho YJ, Yen RF. Comparison and discrepancy of 18F-2-deoxyglucose positron emission tomography and Tc-99m MDP bone scan to detect bone metastases. *Anticancer Res* 2000; **20**: 2189–2192.

55 Katayama T, Kubota K, Machida Y, Toriihara A, Shibuya H. Evaluation of sequential FDG-PET/CT for monitoring bone metastasis of breast cancer during therapy: correlation between morphological and metabolic changes with tumor markers. *Ann Nucl Med* 2012; **26**: 426–435

56 Simoncic U, Perlman S, Liu G, Staab MJ, Straus JE, Jeraj R. Comparison of NaF and FDG PET/CT for assessment of treatment response in castration-resistant prostate cancers with osseous metastases. *Clin Genitourin Cancer* 2015; **13**: e7–e17.

57 Morris MJ, Akhurst T, Larson SM *et al.* Fluorodeoxyglucose positron emission tomography as an outcome measure for castrate metastatic prostate cancer treated with antimicrotubule chemotherapy. *Clin Cancer Res* 2005; **11**: 3210–3216.

58 Jadvar H. Prostate cancer: PET with 18F-FDG, 18F- or 11C-acetate, and 18F- or 11C-choline. *J Nucl Med* 2011; **52**: 81–89.

59 Lebtahi R, Cadiot G, Delahaye N *et al.* Detection of bone metastases in patients with endocrine gastroenteropancreatic tumors: bone scintigraphy compared with somatostatin receptor scintigraphy. *J Nucl Med* 1999; **40**: 1602–1608.

60 Mojtahedi A, Thamake S, Tworowska I, Ranganathan D, Delpassand ES. The value of (68)Ga-DOTATATE PET/CT in diagnosis and management of neuroendocrine tumors compared to current FDA approved imaging modalities: a review of literature. *Am J Nucl Med Mol Imaging* 2014; **4**: 426–434.

61 Osborne JR, Green DA, Spratt DE *et al.* A prospective pilot study of (89)Zr-J591/prostate specific membrane antigen positron emission tomography in men with localized prostate cancer undergoing radical prostatectomy. *J Urol* 2014; **191**: 1439–1445.

62 Szabo Z, Mena E, Rowe SP *et al.* Initial evaluation of [F]DCFPyL for prostate-specific membrane antigen (PSMA)-targeted PET imaging of prostate cancer. *Mol Imaging Biol* 2015 Apr 21. [Epub ahead of print]

63 Afshar-Oromieh A, Malcher A, Eder M *et al.* PET imaging with a [68Ga]gallium-labelled PSMA ligand for the diagnosis of prostate cancer: biodistribution in humans and first evaluation of tumour lesions. *Eur J Nucl Med Mol Imaging* 2013; **40**: 486–495.

64 Perik PJ, Lub-De Hooge MN, Gietema JA *et al.* Indium-111-labeled trastuzumab scintigraphy in patients with human epidermal growth factor receptor 2-positive metastatic breast cancer. *J Clin Oncol* 2006; **24**: 2276–2282.

65 Brouwers AH, Dorr U, Lang O *et al.* 131 I-cG250 monoclonal antibody immunoscintigraphy versus [18 F]FDG-PET imaging in patients with metastatic renal cell carcinoma: a comparative study. *Nucl Med Commun* 2002; **23**: 229–236.

66 Brouwers AH, Buijs WC, Oosterwijk E *et al.* Targeting of metastatic renal cell carcinoma with the chimeric monoclonal antibody G250 labeled with (131)I or (111)In: an intrapatient comparison. *Clin Cancer Res* 2003; **9**: 3953S–3960S.

67 Mankoff DA, Pryma DA, Clark AS. Molecular imaging biomarkers for oncology clinical trials. *J Nucl Med* 2014; **55**: 525–528.

68 O'Connor JP, Jackson A, Asselin MC, Buckley DL, Parker GJ, Jayson GC. Quantitative imaging biomarkers in the clinical development of targeted therapeutics: current and future perspectives. *Lancet Oncol* 2008; **9**: 766–776.

69 Strimbu K, Tavel JA. What are biomarkers? *Curr Opin HIV AIDS* 2010; **5**: 463–466.

70 Therasse P, Arbuck SG, Eisenhauer EA *et al.* New guidelines to evaluate the response to treatment in solid tumors. European Organization for Research and Treatment of Cancer, National Cancer Institute of the United States, National Cancer Institute of Canada. *J Natl Cancer Inst* 2000; **92**: 205–216.

71 Imbriaco M, Larson SM, Yeung HW *et al.* A new parameter for measuring metastatic bone involvement by prostate cancer: the Bone Scan Index. *Clin Cancer Res* 1998; **4**: 1765–1772.

72 Wakabayashi H, Nakajima K, Mizokami A *et al.* Bone scintigraphy as a new imaging biomarker: the relationship between bone scan index and bone metabolic markers in prostate cancer patients with bone metastases. *Ann Nucl Med* 2013; **27**: 802–807.

73 Ulmert D, Kaboteh R, Fox JJ *et al.* A novel automated platform for quantifying the extent of skeletal tumour involvement in prostate cancer patients using the Bone Scan Index. *Eur Urol* 2012; **62**: 78–84.

74 Pierce TP, Jauregui JJ, Cherian JJ, Elmallah RK, Mont MA. Imaging evaluation of patients with osteonecrosis of the femoral head. *Curr Rev Musculoskelet Med* 2015 Jun 5. [Epub ahead of print]

75 Maas O, Joseph GB, Sommer G, Wild D, Kretzschmar M. Association between cartilage degeneration and subchondral bone remodeling in patients with knee osteoarthritis comparing MRI and Tc-DPD-SPECT/CT. *Osteoarthritis Cartilage* 2015 May 29. doi: 10.1016/j.joca.2015.05.014. [Epub ahead of print]

76 Ha S, Hong SH, Paeng JC *et al.* Comparison of SPECT/CT and MRI in diagnosing symptomatic lesions in ankle and foot pain patients: diagnostic performance and relation to lesion type. *PLoS One* 2015; **10**: e0117583.

77 Segall G, Delbeke D, Stabin MG *et al.* SNM practice guideline for sodium 18F-fluoride PET/CT bone scans 1.0. *J Nucl Med* 2010; **51**: 1813–1820.

78 Schirrmeister H. Detection of bone metastases in breast cancer by positron emission tomography. *Radiol Clin North Am* 2007; **45**: 669–676, vi.

79 Muzahir S, Jeraj R, Liu G *et al.* Differentiation of metastatic vs degenerative joint disease using semi-quantitative analysis with (18) F-NaF PET/CT in castrate resistant prostate cancer patients. *Am J Nucl Med Mol Imaging* 2015; **5**: 162–168.

80 Vogel CL, Schoenfelder J, Shemano I, Hayes DF, Gams RA. Worsening bone scan in the evaluation of antitumor response during hormonal therapy of breast cancer. *J Clin Oncol* 1995; **13**: 1123–1128.

81 Rossleigh MA, Lovegrove FT, Reynolds PM, Byrne MJ, Whitney BP. The assessment of response to therapy of bone metastases in breast cancer. *Aust N Z J Med* 1984; **14**: 19–22.

82 van Schelven WD, Pauwels EK. The flare phenomenon: far from fair and square. *Eur J Nucl Med* 1994; **21**: 377–380.

83 Pollen JJ, Witztum KF, Ashburn WL. The flare phenomenon on radionuclide bone scan in metastatic prostate cancer. *AJR Am J Roentgenol* 1984; **142**: 773–776.

84 McNamara MA, George DJ. Pain, PSA flare, and bone scan response in a patient with metastatic castration-resistant prostate cancer treated with radium-223, a case report. *BMC Cancer* 2015; **15**: 371.
85 Cook GJ, Venkitaraman R, Sohaib AS *et al.* The diagnostic utility of the flare phenomenon on bone scintigraphy in staging prostate cancer. *Eur J Nucl Med Mol Imaging* 2011; **38**: 7–13.
86 Schneider JA, Divgi CR, Scott AM *et al.* Flare on bone scintigraphy following Taxol chemotherapy for metastatic breast cancer. *J Nucl Med* 1994; **35**: 1748–1752.
87 Chao HS, Chang CP, Chiu CH, Chu LS, Chen YM, Tsai CM. Bone scan flare phenomenon in non-small-cell lung cancer patients treated with gefitinib. *Clin Nucl Med* 2009; **34**: 346–349.
88 Gillespie PJ, Alexander JL, Edelstyn GA. Changes in 87mSr concentractions in skeletal metastases in patients responding to cyclical combination chemotherapy for advanced breast cancer. *J Nucl Med* 1975; **16**: 191–193.
89 Sugawara Y, Kajihara M, Semba T, Ochi T, Fujii T, Mochizuki T. Healing focal ''flare'' phenomenon after radiotherapy in a bone metastasis from bladder cancer. *Clin Nucl Med* 2005; **30**: 672–673.
90 Cheng TH, Holman BL. Increased skeletal:renal uptake ratio: etiology and characteristics. *Radiology* 1980; **136**: 455–459.
91 Swislocki AL, Barnett CA, Darnell P, Noth RH. Hyperthyroidism: an underappreciated cause of diffuse bone disease. *Clin Nucl Med* 1998; **23**: 241–243.
92 Ell PJ. The contribution of PET/CT to improved patient management. *Br J Radiol* 2006; **79**: 32–36.
93 Scher HI, Halabi S, Tannock I *et al.* Design and end points of clinical trials for patients with progressive prostate cancer and castrate levels of testosterone: recommendations of the Prostate Cancer Clinical Trials Working Group. *J Clin Oncol* 2008; **26**: 1148–1159.
94 Lee RJ, Saylor PJ, Michaelson MD *et al*. A dose-ranging study of cabozantinib in men with castration-resistant prostate cancer and bone metastases. *Clin Cancer Res* 2013; **19**: 3088–3094.
95 Fay AP, Albiges L, Bellmunt J. Current role of cabozantinib in metastatic castration-resistant prostate cancer. *Expert Rev Anticancer Ther* 2015; **15**: 151–156.
96 Doran MG, Spratt DE, Wongvipat J *et al.* Cabozantinib resolves bone scans in tumor-naive mice harboring skeletal injuries. *Mol Imaging* 2014; **13**. doi: 10.2310/7290.2014.00026.
97 Gentili A, Miron SD, Bellon EM. Nonosseous accumulation of bone-seeking radiopharmaceuticals. *Radiographics* 1990; **10**: 871–881.
98 Cerci SS, Suslu H, Cerci C *et al.* Different findings in Tc-99m MDP bone scintigraphy of patients with sickle cell disease: report of three cases. *Ann Nucl Med* 2007; **21**: 311–314.
99 Loutfi I, Collier BD, Mohammed AM. Nonosseous abnormalities on bone scans. *J Nucl Med Technol* 2003; **31**: 149–153; quiz 154–146.
100 Zhang H, Huang R, Cheung NK *et al.* Imaging the norepinephrine transporter in neuroblastoma: a comparison of [18F]-MFBG and 123I-MIBG. *Clin Cancer Res* 2014; **20**: 2182–2191.
101 Beekman FJ, van der Have F, Vastenhouw B *et al.* U-SPECT-I: a novel system for submillimeter-resolution tomography with radiolabeled molecules in mice. *J Nucl Med* 2005; **46**: 1194–1200.
102 Beekman F, van der Have F. The pinhole: gateway to ultra-high-resolution three-dimensional radionuclide imaging. *Eur J Nucl Med Mol Imaging* 2007; **34**: 151–161.
103 Torigian DA, Zaidi H, Kwee TC *et al.* PET/MR imaging: technical aspects and potential clinical applications. *Radiology* 2013; **267**: 26–44.
104 Hofmann M, Pichler B, Scholkopf B, Beyer T. Towards quantitative PET/MRI: a review of MR-based attenuation correction techniques. *Eur J Nucl Med Mol Imaging* 2009; **36**: S93–S104.
105 Jadvar H, Colletti PM. Competitive advantage of PET/MRI. *Eur J Radiol* 2014; **83**: 84–94.